Journal of Sound and Vibration (1999) **223**(1), 73–95
Article No. jsvi.1998.2137, available online at http://www.idealibrary.com on IDEAL®

ASYMPTOTIC FORMULATION FOR AN ACOUSTICALLY DRIVEN FIELD INSIDE A RECTANGULAR CAVITY WITH A WELL-DEFINED CONVECTIVE MEAN FLOW MOTION

J. MAJDALANI
Department of Mechanical and Industrial Engineering, Marquette University,
1515 *West Wisconsin Avenue, Milwaukee, WI* 53233, *U.S.A.*

(*Received* 10 *July* 1998, *and in final form* 11 *December* 1998)

When small amplitude harmonic pressure waves are introduced inside an enclosure where the classic cavity flow is already established, a strong coupling ensues between the mean and time-dependent fields. In addition to the mean flow influence, the presence of solid boundaries gives rise to a strong coupling between acoustic and vortical waves that prescribes the propagation of disturbances. Based on a well-defined mean flow structure, the purpose of this report is to arrive at closed-form expressions for the two-dimensional, time-dependent velocity and vorticity fields, in order to elucidate the nature and extent of intrinsic flow coupling. On that account, regular perturbation tools are used on the vorticity transport equation derived from the linearised Navier–Stokes equations. After an inviscid expansion is achieved, successive approximations that use viscous correction multipliers are employed to derive the vorticity in a manner to satisfy the existing boundary conditions. At the outset, unsteady vorticity is found to originate at the walls due to the acoustic pressure gradient normal to the inflow direction. In consequence, most intense vortices are initiated in regions that coincide with acoustic pressure nodes. Conversely, zero vorticity streaks emanate from acoustic velocity nodes and are carried downstream by the bulk fluid motion. From the vorticity formulation, both components of the time-dependent velocity vector are derived in a manner to satisfy continuity and momentum conservation. The axial velocity component is found to be the most significant, exhibiting characteristics associated with oscillatory flows. In addition to comparisons with numerical simulations, a limiting process validation against the existing exact solution in the event of no mean flow transmission is carried out. In closing, an error assessment is included to quantify both magnitude and order of the global error accumulated in the final asymptotic expressions.

© 1999 Academic Press

1. INTRODUCTION

When a well-prescribed steady flow field inside an enclosure is subjected to time-harmonic pressure oscillations, a complex time-dependent environment is established. The purpose of this paper is to analyse the resulting field which is

0022–460X/99/210073 + 23 $30.00/0 © 1999 Academic Press

the outcome of a strong interaction between the convective mean flow motion and the ensuing acoustic and vortical waves. The latter are formed, evidently, by virtue of the oscillatory pressure gradients normal to mean flow streamlines. The time-dependent environment produced by such interactions exhibit conventional aspects predicted by classic theories in addition to new and compelling features that will be elucidated in the current report.

In order to manage a closed-form solution for the closely intertwined velocity and vorticity fields, several reasonable idealisations will be effectuated. For example, the low geometric aspect ratio of the cavity's cross-sectional area will be exploited to justify ignoring variations in one spatial direction. Symmetry of a well-behaved flow about the cavity's core will also be invoked to reduce the solution domain by half. In order to break down the remaining task into digestible pieces, the resulting two-dimensional, time-dependent field will be decomposed into steady and time-dependent components. Based on small amplitude pressure oscillations, the Navier–Stokes equations are then linearised in a manner to provide the conservation of mass and momentum equations for the coupled field written to the first order in the normalised pressure wave amplitude.

While the steady field equations can be easily satisfied by a well-defined mean flow solution inside a cavity, the search for a time-dependent field that satisfies the linearised equations—burdened by the mean flow influence—constitutes the main goal of this theoretical investigation. The strategy will be to proceed carefully, using known mathematical theorems and regular perturbation tools, in order to extract meaningful, uniformly valid expressions for the dependent variables. For instance, the time-dependent velocity vector will be decomposed into an irrotational, acoustic component, and a rotational, solenoidal counterpart. The interaction equations will be derived for each set and their solutions will be superimposed in a way to satisfy existing boundary conditions. While the solution to the acoustic set can be concocted without much difficulty, the vortical set requires much effort and will be presented in detail in a separate section devoted to the mathematical treatment. At the heart of the analysis will be the manipulation of the linearised vorticity transport equation which will be solved using separation of variables. Successive approximation concepts will be necessitated in reaching a zeroth-order inviscid formulation based on which a viscous correction will be constructed. The final formulations that reveal the key controlling parameters will be described and compared to numerical solutions of the governing differential equations of motion. The acoustico-vortical structure will also be characterised. Since an exact solution exists for the same geometry and time-harmonic pressure oscillations in the absence of a mean flow, the asymptotic results will be compared to the exact predictions in the limiting process when the normal convection speed is reduced below the Stokes diffusion speed. A standard error analysis will also be furnished to quantify both magnitude and order of the maximum truncation error incurred in the derivation process.

The scientific merit of this work rests in the somewhat original small parameter perturbation treatment of the linearised Navier–Stokes equations, in

addition to the disclosure of novel aspects of pertinent acoustico-vortical structures revealed by the finite asymptotic expressions. Practical applications include cold flow experiments that incorporate an acoustic motion over transpiring surfaces in rectangular cavities. At the time of this writing, the author is familiar with two experimental investigations that simulate the oscillatory flow over transpiring surfaces including a sinusoidal wave motion parallel to the transpiring surface. The reader is referred to, in that regard, to the works of Ma *et al.* [1–3] and Barron *et al.* [4, 5] who used sublimating carbon dioxide that originates from flat blocks of dry ice to simulate the transpiring gas inside a long, segmented, rectangular chamber. The main difference between both experimental apparatuses lies in the choice of a wave generator. While Ma's source of acoustic waves consisted of a reciprocating piston controlled by a variable speed, slider-crank mechanism, Barron's apparatus used a Scotch-yoke mechanism that produced purer sinusoidal piston motions. Since both experimental investigations were conducted in the absence of applicable theoretical models, the results of this study are hoped to provide an alternative for drawing experimental comparisons.

2. SYSTEM

The analysis starts by defining the solution domain and accompanying solid boundaries. In the process, the main criteria that must hold true for the model to be valid are stated as well.

2.1. SOLUTION DOMAIN

Prior to the onset of acoustic oscillations, the classic two-dimensional cavity mean flow field is considered inside a rectangular enclosure of length L, width W, and height $2H$ ($W \gg H$, $L \gg H$). Due to symmetry, only half of the enclosure is shown in Figure 1 where y and z are used to denote the vertical and axial co-ordinates normalised by H. In order to admit the inflow of gas, the top wall ($y = 1$) is made permeable to simulate a transpiring surface. As a result, choked streams of gas of kinematic viscosity v_0 are allowed to enter the enclosure with a normal blowing speed component V_b. As gas streams swerve and head downstream, they prescribe the bulk fluid motion represented by the streamlines depicted in Figure 1. Except for the top wall and the outflow section, all other boundaries are impenetrable. In order to simulate practical flows that incorporate a nozzle section at the downstream end, the outflow section is assumed to correspond to a choked area. In seeking two-dimensional solutions, it is only appropriate to consider enclosures whose width exceeds their height in order to justify ignoring variations in the x direction. Due to symmetry about the core ($y = 0$) the solution domain is limited on the interval $0 \leqslant y \leqslant 1$. In addition, coupling with acoustic disturbances is to be considered when harmonic pressure oscillations of small amplitude A_p are introduced at a circular frequency ω_0. This acoustic environment can be either induced externally or triggered naturally depending on the application.

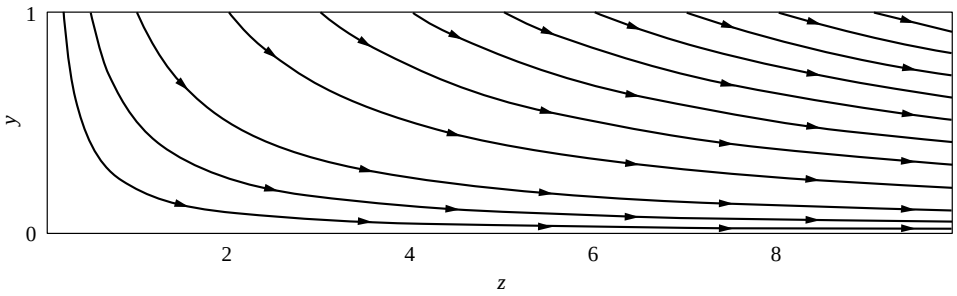

Figure 1. Solution domain including mean flow streamlines.

2.2. ORIGINAL PREMISES

As it will become apparent in the forthcoming analysis, in order to achieve an asymptotic solution to the time-dependent field, the presence of several relatively small parameters is exploited. The first is the normal inflow Mach number, V_b/c, where c happens to be the intrinsic speed of sound inside the cavity. In the current report, physical settings with a Mach number of $O(10^{-3})$ will be considered. In practical non-reacting flows characterised by $c \cong 350$ m/s, the low Mach number criterion is not prohibitive.

Another basic premise that must remain valid limits the acoustic pressure amplitude A_p to remain small by comparison to the mean pressure p_0 at $z = 0$. This is necessitated by the requirement of a small pressure wave amplitude, A_p/p_0, which will be used as a primary perturbation parameter in linearising the Navier–Stokes equation.

Finally, in order to maintain consistency in perturbation orders, the mean pressure distribution will need to be as uniform as possible. This, of course, is dictated by the mean flow character. In the present work, this somewhat "flexible" condition casts an approximate limit on the length of the cavity, namely, $L/H < 100$. When these criteria are met, the following analysis can be appropriate everywhere in the absence of fully developed turbulence and flow separation.

3. GOVERNING EQUATIONS

3.1. CONSERVATION LAWS

The Navier–Stokes equations can be cast in dimensionless form into

$$\frac{\partial \rho}{\partial t} + \nabla \cdot (\rho \mathbf{u}) = 0, \tag{1}$$

$$\rho \frac{\mathrm{D}\mathbf{u}}{\mathrm{D}t} = -\frac{\nabla p}{\gamma} + \frac{1}{Re}\left[\frac{4}{3}\nabla(\nabla \cdot \mathbf{u}) - \nabla \times (\nabla \times \mathbf{u})\right], \tag{2}$$

when body forces are ignored, viscosity is assumed to be uniform, and the bulk viscosity is neglected. In writing the set, density and pressure are normalised by

their mean values, ρ_0 and p_0, at $z = 0$, velocities are normalised by c, spatial co-ordinates are normalised by H, and time is made dimensionless by reference to the average time it takes for a pressure disturbance to travel from the wall to the core, (H/c). The Reynolds number Re in equation (2) is (cH/v_0), γ is the ratio of specific heats, and $\mathbf{u}(y, z, t)$ is the total velocity vector. Extruding $\mathbf{u}(y, z, t)$ constitutes the main purpose of this report.

3.2. STRATEGY

First, the internal flow field is decomposed into steady and time-dependent parts. This is accomplished by writing the independent variables as sums of their steady and time-dependent components. Small parameter perturbations are ideally suited because of the fundamental premise requiring the acoustic amplitude to remain small [6]. In splitting the field, it is assumed that the presence of time-dependent oscillations does not alter the bulk fluid motion. This assumption can be later verified by realising that terms that incorporate the time-dependent effects on the mean flow are indeed secondary. In contrast, mean flow effects on the acoustic field cannot be dismissed since their incorporation is behind the distinguishing features of the resulting particle motion.

3.3. STEADY AND TIME-DEPENDENT VARIABLES

Using asterisks to denote dimensional variables, and superscripts for perturbation orders, the dimensional pressure can be expressed as

$$p^* = p^{*(0)}(y^*, z^*) + p^{*(1)}(y^*, z^*, t^*) = p^{*(0)} + A_p f(y^*, z^*) \cos(\omega_0 t^*), \tag{3}$$

where $p^{*(0)}$, subject to later verification, is taken here to be a constant: $p^{*(0)} \cong p_0$. In the time-dependent part of equation (3), f is a normalised spatial function of the order of unity. When normalised by p_0, equation (3) becomes

$$p = 1 + \varepsilon_w f(y, z) \cos(\omega_0 t^*) = 1 + p^{(1)}(y, z, t), \tag{4}$$

where $\varepsilon_w = A_p/p_0$ is the primary perturbation parameter to which other quantities can be compared. Density can be expanded in a similar way:

$$\rho(y, z, t) = \frac{\rho_0 + \rho^{*(1)}}{\rho_0} = 1 + \rho^{(1)}(y, z, t). \tag{5}$$

Velocity decomposition is assessed slightly differently since its mean value is of the order of $V_b\mathbf{U}(y, z)$, where $\mathbf{U}(y, z)$ is a function of $O(1)$ to be discussed in section 4. After expanding the velocity into

$$\mathbf{u}^*(y, z, t) = V_b\mathbf{U}(y, z) + \mathbf{u}^{*(1)}(y, z, t), \tag{6}$$

normalise by c and get

$$\mathbf{u}(y, z, t) = M_b\mathbf{U}(y, z) + \mathbf{u}^{(1)}(y, z, t), \tag{7}$$

where the wall Mach number appears as a secondary perturbation parameter by virtue of $\varepsilon_w < M_b \ll 1$.

3.4. STEADY AND TIME-DEPENDENT EQUATIONS

When equations (4), (5) and (7) are substituted back into equations (1) and (2), a set is obtained to $O(\varepsilon_w^0 \equiv 1)$ that governs the steady flow motion:

$$\nabla \cdot \mathbf{U} = 0, \quad \mathbf{U} \cdot \nabla \mathbf{U} = \frac{1}{M_b Re}\left[\frac{4}{3}\nabla(\nabla \cdot \mathbf{U}) - \nabla \times (\nabla \times \mathbf{U})\right]. \tag{8, 9}$$

When terms that are of $O(\varepsilon_w)$ are collected, a linearised expansion of the conservation of mass and momentum equations is attained (see Appendix A for details):

$$\partial \rho^{(1)}/\partial t + \nabla \cdot \mathbf{u}^{(1)} = -M_b \nabla \cdot (\rho^{(1)}\mathbf{U}), \tag{10}$$

$$\frac{\partial \mathbf{u}^{(1)}}{\partial t} = M_b[\mathbf{u}^{(1)} \times (\nabla \times \mathbf{U}) + \mathbf{U} \times (\nabla \times \mathbf{u}^{(1)}) - \nabla(\mathbf{u}^{(1)} \cdot \mathbf{U})] - \frac{\nabla p^{(1)}}{\gamma} + \frac{1}{Re}\left[\frac{4}{3}\nabla(\nabla \cdot \mathbf{u}^{(1)}) - \nabla \times (\nabla \times \mathbf{u}^{(1)})\right]. \tag{11}$$

These linearised equations reveal the intricate coupling between mean and time-dependent fields which strongly influence the total time-dependent solution character.

4. MEAN FLOW CHARACTER

4.1. VELOCITY FIELD

The steady velocity vector $\mathbf{U}$ can be determined from the stream function $\mathbf{S}_f = \Psi \mathbf{e}_x$ defined for a flow inside a rectangular cavity [7] where $\mathbf{U} = \nabla \times \mathbf{S}_f$. In actuality, the classical stream function $\Psi(y, z) = -yz$, whose streamlines are shown in Figure 1, begets

$$\mathbf{U} = U_y \mathbf{e}_y + U_z \mathbf{e}_z = \frac{\partial \Psi}{\partial z}\mathbf{e}_y - \frac{\partial \Psi}{\partial y}\mathbf{e}_z = -y\mathbf{e}_y + z\mathbf{e}_z, \tag{12}$$

which satisfies equations (8) and (9).

4.2. PRESSURE CORRECTION

Having already defined the velocity field, the steady momentum equation can be used to deduce the pressure associated with the resulting mean flow. Without suffering any loss in generality, pressure can be expanded as $p(y, z, t) = 1 + p_c(y, z) + p^{(1)}(y, z, t)$, where $p_c(y, z)$ is a spatial pressure correction term that we propose to determine. A boundary condition that must be met demands that pressure at $z = 0$ be identical to the mean stagnation pressure p_0; this signifies that $p^{(0)}(0, 0) = 1 + p_c(0, 0) = 1$, or $p_c(0, 0) = 0$. The pertinent spatial correction $p_c(y, z)$ can be obtained from equation (2) by direct substitution:

$$M_b\mathbf{U}\cdot\nabla(N_b\mathbf{U}) = -\frac{\nabla p_c}{\gamma} + \frac{1}{Re}\left[\frac{4}{3}\nabla[\nabla\cdot(M_b\mathbf{U})] - \nabla\times[\nabla\times(M_b\mathbf{U})]\right], \tag{13}$$

or

$$\nabla p_c/(\gamma M_b^2) = -\mathbf{U}\cdot\nabla\mathbf{U}, \tag{14}$$

which can be integrated to obtain, for $p_c(0, 0) = 0$, $p^{(0)}(y, z) = 1 - \frac{\gamma}{2} M_b^2(y^2 + z^2)$; finally,

$$p^{(0)}(y, z) = 1 - \frac{\gamma}{2} M_b^2(y^2 + z^2). \tag{15}$$

Equation (15) clearly indicates that spatial variations in pressure are secondary, being of order $M_b^2 z^2$. As long as $z < 100$, the error incurred by disregarding spatial variations remains less than 1% since M_b is of $O(10^{-3})$. The corrected pressure distribution confirms that axial pressure variations are indeed negligible except in very long chambers with large Mach numbers.

5. TIME-DEPENDENT FIELD SYNTHESIS

5.1. PRESSURE AND VORTICITY FIELDS

The time-dependent velocity vector representing small amplitude disturbances can be decomposed into two vectors of distinct characters [8]: one that is acoustic or irrotational, and one that is vortical or solenoidal. Designating the irrotational mode variables by the circumflex (ˆ), and the solenoidal variables by the tilde (˜), one can synthesise the velocity vector from

$$\mathbf{u}^{(1)} = \mathbf{u}_{\text{irrotational}} + \mathbf{u}_{\text{solenoidal}} = \hat{\mathbf{u}} + \tilde{\mathbf{u}}, \tag{16}$$

contingent upon $\nabla\times\hat{\mathbf{u}} = 0$, and $\nabla\cdot\tilde{\mathbf{u}} = 0$. Similar decomposition of small amplitude disturbances into two modes of fluctuations, an acoustic or pressure mode and a solenoidal or vorticity mode, has been accomplished routinely in the literature. The reader is referred to, for instance, the works of Chu and Kovásznay [9] or Flandro [10].

When equation (16) is plugged back into equations (10) and (11), interaction equations for small amplitude fluctuations can be expressed for each of the modes. In the process, time-dependent expressions for vorticity, pressure, and density appear. These quantities are

$$\boldsymbol{\omega}^{(1)} \equiv \nabla\times\mathbf{u}^{(1)} = \tilde{\boldsymbol{\omega}} \equiv \nabla\times\tilde{\mathbf{u}}, \tag{17}$$

$$p^{(1)} = \hat{p}, \quad \rho^{(1)} = \hat{\rho}, \tag{18, 19}$$

where vorticity is seen to be produced exclusively by the rotational mode and time-dependent pressure is caused by the acoustic mode. The pseudo-pressure associated with the vorticity mode is ignored, being of second order in the wave amplitude [9].

5.2. TIME-DEPENDENT EQUATIONS OF MOTION

Substitution of equations (16)–(19) into the linearised Navier–Stokes set, given by equations (10) and (11), begets two independent sets of partial differential equations that govern the acoustic and vortical wave motions.

5.2.1. *Acoustical model*

$$\partial\hat{\rho}/\partial t + \nabla\cdot\hat{\mathbf{u}} = -M_b\nabla\cdot(\hat{\rho}\mathbf{U}), \tag{20}$$

$$\frac{\partial\hat{\mathbf{u}}}{\partial t} = -\frac{\nabla\hat{p}}{\gamma} - M_b\nabla(\hat{\mathbf{u}}\cdot\mathbf{U}) + \frac{4\nabla(\nabla\cdot\hat{\mathbf{u}})}{3Re}. \tag{21}$$

5.2.2. *Vortical model*

$$\nabla\cdot\tilde{\mathbf{u}} = 0, \tag{22}$$

$$\frac{\partial\tilde{\mathbf{u}}}{\partial t} = M_b[\mathbf{U}\times\tilde{\boldsymbol{\omega}} - \nabla(\tilde{\mathbf{u}}\cdot\mathbf{U})] - \frac{\nabla\times\tilde{\boldsymbol{\omega}}}{Re}. \tag{23}$$

5.3. BOUNDARY CONDITIONS

In order to evaluate $\mathbf{u}^{(1)} = \hat{\mathbf{u}} + \tilde{\mathbf{u}}$, irrotational and vortical components must first be determined separately by solving equations (20) and (21), and equations (22) and (23), respectively. Resulting solutions must be juxtaposed in a manner to correctly satisfy the existing boundary conditions. These include (1) the no-slip condition at the wall requiring the axial time-dependent component of the velocity to vanish at $y = 1$, thus yielding $\tilde{u}_z(1, z) = -\hat{u}_z(1, z)$; and (2) symmetry at $y = 0$, translating into $\partial u^{(1)}(0, z)/\partial y = 0$.

5.4. ACOUSTIC SOLUTION

Equations (20) and (21) can be rearranged into a set that possesses a classic solution presented in most texts on acoustics. This is accomplished by manipulating equations (20) and (21) to eliminate one of the two dependent variables. When $\hat{\mathbf{u}}$ is eliminated out, the ensuing PDE is

$$\frac{\partial^2\hat{p}}{\partial t^2} - \nabla^2\hat{p} = -M_b\left[\nabla\cdot\left(\frac{\partial\hat{p}}{\partial t}\mathbf{U}\right) + \gamma\nabla^2(\hat{\mathbf{u}}\cdot\mathbf{U})\right]. \tag{24}$$

Clearly, equation (24) can be solved to $O(M_b)$ by separation of variables. Since our enclosure is characterised by $H/L \ll 1$, transverse oscillation modes can be ignored, and one is left with the classic one-dimensional solution to equation (24). Expressed in complex variable notation,

$$\hat{p}(z, t) = \varepsilon_w\cos(k_m z)\exp(-\mathrm{i}k_m t), \tag{25}$$

where the wave number is given by $k_m = m\pi H/L$, $m = 1, 2, 3, \ldots$, and m is the acoustic oscillation mode number. The acoustic velocity companion can be determined directly from equation (21). The result, to $O(M_b)$, is

$$\hat{\mathbf{u}}(z, t) = \mathrm{i}\frac{\varepsilon_w}{\gamma}\sin(k_m z)\exp(-\mathrm{i}k_m t)\mathbf{e}_z. \tag{26}$$

5.5. VORTICAL EQUATIONS

Maintaining Euler's notation for algebraic convenience, the rotational velocity and vorticity components can be expressed as

$$\tilde{\mathbf{u}}(y, z, t) = \mathbf{V}(y, z)\exp(-\mathrm{i}k_m t), \quad \tilde{\boldsymbol{\omega}}(y, z, t) = \boldsymbol{\varpi}(y, z)\exp(-\mathrm{i}k_m t), \tag{27, 28}$$

where

$$\mathbf{V}(y, z) = V_y\mathbf{e}_y + V_z\mathbf{e}_z, \quad \boldsymbol{\varpi} = \nabla\times\mathbf{V} = \varpi\mathbf{e}_x. \tag{29, 30}$$

When these benign variable transformations are implemented, the vortical mass and momentum conservation equations, given by equations (22) and (23), become

$$\nabla\cdot\mathbf{V} = 0, \quad \mathrm{i}\mathbf{V} = \sigma[\nabla(\mathbf{V}\cdot\mathbf{U}) - \mathbf{U}\times\boldsymbol{\varpi}] + \varepsilon\nabla\times\boldsymbol{\varpi}, \tag{31, 32}$$

where

$$\sigma = \frac{M_b}{k_m} = \frac{1}{Sr} = \frac{V_b}{\omega_0 H} < O(10^{-1}), \tag{33}$$

$$\varepsilon = \frac{1}{k_m Re} = \frac{1}{Re_k} = \left(\sqrt{\frac{\nu_0/\omega_0}{H}}\right)^2 < O(10^{-4}), \tag{34}$$

are the reciprocals of the Strouhal and kinetic Reynolds numbers. Notably, $\varepsilon \ll \sigma \ll 1$, since

$$\varepsilon/\sigma = \nu_0/(V_b H) \ll 1. \tag{35}$$

Having defined the dynamic similarity parameters in control of the linearised vortical equations, equations (31) and (32) can be expanded in scalar form into

$$\frac{\partial V_y}{\partial y} + \frac{\partial V_z}{\partial z} = 0, \tag{36}$$

$$\mathrm{i}V_y = \sigma\left[\frac{\partial}{\partial y}(V_y U_y) + U_z\frac{\partial V_y}{\partial z} + V_z\frac{\partial U_y}{\partial z}\right] - \varepsilon\left(\frac{\partial^2 V_y}{\partial z^2} - \frac{\partial^2 V_z}{\partial y\partial z}\right), \tag{37}$$

$$\mathrm{i}V_z = \sigma\left[\frac{\partial}{\partial z}(V_z U_z) + U_y\frac{\partial V_z}{\partial y} + V_y\frac{\partial U_z}{\partial y}\right] - \varepsilon\left(\frac{\partial^2 V_z}{\partial y^2} - \frac{\partial^2 V_y}{\partial y\partial z}\right). \tag{38}$$

These reveal that direct analytical solutions to the coupled set are nearly

impossible unless one exploits a key result that can be verified numerically, and proven theoretically, only *a posteriori*. This result, which will be later verified, asserts that the normal vortical velocity amplitude is of $O(M_b)$ by comparison to the axial component. Being a smaller quantity, ignoring V_y will not affect the solution which, let us recall, is only accurate to $O(M_b)$. At the outset, equation (38) becomes

$$\mathrm{i}V_z = \sigma\left[\frac{\partial}{\partial z}(V_z U_z) + U_y\varpi\right] - \varepsilon\frac{\partial\varpi}{\partial y} + O(M_b). \tag{39}$$

6. VORTICAL SOLUTION

Using regular perturbations, the conservation principles presented above can be coupled with the vorticity transport equation to extrude an explicit solution to the solenoidal velocity and vorticity vectors.

6.1. FORMULATION

To produce the vorticity transport equation associated with the solenoidal field, take the curl of equation (32), and use equation (30); the outcome is

$$\mathrm{i}\boldsymbol{\varpi} = -\sigma\nabla\times(\mathbf{U}\times\boldsymbol{\varpi}) - \varepsilon\nabla^2\boldsymbol{\varpi}. \tag{40}$$

Equation (40) can be expressed in scalar terms and rearranged to group leading order terms on the left-hand side; when this is done, one gets

$$\frac{\partial\varpi}{\partial y} - \frac{\mathrm{i}\varpi}{\sigma U_y} + \frac{U_z}{U_y}\frac{\partial\varpi}{\partial z} = \frac{\varepsilon}{\sigma U_y}\left(\frac{\partial^2\varpi}{\partial y^2} + \frac{\partial^2\varpi}{\partial z^2}\right). \tag{41}$$

In order to justify ignoring the viscous diffusion of unsteady vorticity—represented by the right-hand side of equation (41)—at the first perturbation level, a variable transformation $Y = y/M_b$ is introduced, whose action is to stretch the normal scale over the Mach number range. When this is executed, equation (41) becomes

$$\frac{\partial\varpi}{\partial Y} - \frac{\mathrm{i}k_m\varpi}{U_y} + M_b\frac{U_z}{U_y}\frac{\partial\varpi}{\partial z} = \frac{1}{ReU_y}\left(\frac{1}{M_b^2}\frac{\partial^2\varpi}{\partial Y^2} + \frac{\partial^2\varpi}{\partial z^2}\right), \tag{42}$$

which indicates that the right-hand side of equation (42) contains smaller order terms; at the outset, it can be argued that subsequent zeroth-order perturbation expansions in the Mach number will not be affected by their presence. The third term on the left-hand side is retained, despite its misleading appearance of $O(M_b)$, because it represents the downstream convection of vorticity, which is vital to preserve two-dimensionality. Being a function of the axial co-ordinate z, it is essential to satisfy the laws of physics and, mathematically, provide a nontrivial separable solution. The zeroth-order solution can now be achieved in a straightforward fashion by expanding the vorticity in powers of the Mach number, $\varpi = \varpi_0 + M_b\varpi_1 + M_b^2\varpi_2 + O(M_b^3)$, and by substituting the expansion

back into equation (42). It follows that the leading-order term ϖ_0 is obtainable, by separation of variables, from

$$\frac{\partial \varpi_0}{\partial y} - \frac{\mathrm{i}\varpi_0}{\sigma U_y} + \frac{U_z}{U_y}\frac{\partial \varpi_0}{\partial z} = 0. \tag{43}$$

Letting $\varpi_0(y, z) = Y(y)Z(z)$, and recalling equation (12), equation (43) becomes

$$\frac{y}{Y}\frac{\mathrm{d}Y}{\mathrm{d}y} + \frac{\mathrm{i}}{\sigma} = \frac{z}{Z}\frac{\mathrm{d}Z}{\mathrm{d}z} = \lambda_n, \tag{44}$$

where λ_n must be a strictly positive real number for a non-trivial solution. Integrating and summing linearly over all possible solutions yields

$$\varpi_0(y, z) = \exp(-\mathrm{i}\ln y/\sigma)\sum_{\lambda_n} c_n (yz)^{\lambda_n}, \tag{45}$$

where c_n is an integration constant associated with λ_n, which must be determined in a manner to satisfy the no-slip boundary condition at the wall, written for vorticity. The latter requires a delicate treatment and will be addressed separately.

6.2. ACOUSTICALLY GENERATED VORTICITY

Our current state of knowledge allows us to reduce equation (11) into

$$\partial \mathbf{u}^{(1)}/\partial t = -M_b[\nabla(\mathbf{u}^{(1)}\cdot\mathbf{U}) - \mathbf{U}\times\boldsymbol{\omega}^{(1)}] - \nabla p^{(1)}/\gamma - \nabla\times\boldsymbol{\omega}^{(1)}/Re, \tag{46}$$

which, when projected along z, gives

$$\frac{\partial u_z^{(1)}}{\partial t} = -M_b\left[\frac{\partial}{\partial z}(u_y^{(1)}U_y + u_z^{(1)}U_z) + U_y\omega^{(1)}\right] - \frac{1}{\gamma}\frac{\partial p^{(1)}}{\partial z} + \frac{1}{Re}\frac{\partial \omega^{(1)}}{\partial y}. \tag{47}$$

Remarking that $\boldsymbol{\omega}^{(1)} = \tilde{\boldsymbol{\omega}}$, $u_y^{(1)} = \tilde{u}_y$, $p^{(1)} = \hat{p}$, and that $u_z^{(1)}(1, z, t)$ must vanish to prevent slippage, equation (47) becomes, at the wall,

$$0 = -M_b\left[\frac{\partial}{\partial z}(\tilde{u}_y U_y) + U_y\tilde{\omega}\right] - \frac{1}{\gamma}\frac{\partial \hat{p}}{\partial z} + \frac{1}{Re}\frac{\partial \tilde{\omega}}{\partial y}. \tag{48}$$

Rearranging, and using the premise that $\tilde{u}_y/\tilde{u}_z = O(M_b)$, equation (48) becomes

$$-U_y\tilde{\omega} = \frac{1}{\gamma M_b}\frac{\partial \hat{p}}{\partial z} - \frac{\varepsilon}{\sigma}\frac{\partial \tilde{\omega}}{\partial y}, \tag{49}$$

where the acoustic pressure gradient may be derived from $\hat{p} = \varepsilon_w \cos(k_m z)\exp(-\mathrm{i}k_m t)$ to give

$$-U_y\tilde{\omega} = -\frac{\varepsilon_w}{\gamma} Sr \sin(k_m z)\exp(-\mathrm{i}k_m t) - \frac{\varepsilon}{\sigma}\frac{\partial \tilde{\omega}}{\partial y}. \tag{50}$$

Finally, using $U_y(1, z) = -1$ at the wall, and recalling equations (28) and (30), an

expression for the vorticity boundary condition can be obtained,

$$\varpi(1, z) = -\frac{\varepsilon_w}{\gamma} Sr \sin(k_m z) - \frac{\varepsilon}{\sigma}\frac{\partial \varpi}{\partial y}, \tag{51}$$

indicating that "fresh" vorticity is continually generated at the wall by virtue of the local, oscillatory pressure gradient. By comparison to the pressure amplitude, the vorticity amplitude is larger by a factor of $O(Sr)$. This observation, to be verified in the final results, stresses the importance of vortical presence in the acoustically driven coupling.

6.3. INVISCID VORTICITY

Since equation (45) must satisfy equation (51) at $y = 1$, the vorticity boundary condition is utilised to evaluate the separation eigenvalues and corresponding integration constants. This is accomplished by setting

$$\varpi_0(1, z) = -\frac{\varepsilon_w}{\gamma} Sr \sin(k_m z) = -\frac{\varepsilon_w}{\gamma} Sr \sum_{n=0}^{\infty} \frac{(-1)^n (k_m z)^{2n+1}}{(2n+1)!} \equiv \sum_{\lambda_n} c_n z^{\lambda_n} \tag{52}$$

$$\Rightarrow \lambda_n = 2n + 1, \quad n = 0, 1, 2, \ldots, \quad \text{and} \quad c_n = -\frac{\varepsilon_w}{\gamma} Sr \frac{(-1)^n (k_m)^{2n+1}}{(2n+1)!}, \tag{53}$$

wherefrom

$$\varpi_0(y, z) = -\frac{\varepsilon_w}{\gamma} Sr \sin(k_m y z) \exp(-\mathrm{i} Sr \ln y). \tag{54}$$

6.4. INVISCID STREAM FUNCTION

In order to solve for the velocity, the stream function vector, $\mathbf{s}_f = \psi \mathbf{e}_x$, is first introduced which can be employed to eliminate the velocity, $\mathbf{V} \equiv \nabla \times \mathbf{s}_f$, everywhere, by using the stream function equivalent, $V_y = \partial\psi/\partial z$, and $V_z = -\partial\psi/\partial y$. Starting with the vorticity equation,

$$\varpi = \frac{\partial V_z}{\partial y} - \frac{\partial V_y}{\partial z} = -\frac{\partial^2 \psi}{\partial y^2} - \frac{\partial^2 \psi}{\partial z^2}, \tag{55}$$

and realising that ψ must possess the same axial dependence as ϖ, one sets $\psi_0(y, z) = \psi_c(y)\varpi_0(y, z)$, and attempts to solve for the corrective multiplier $\psi_c(y)$ that satisfies equation (55). After some algebra, balancing the leading-order terms results in

$$\psi_c = \sigma^2 y^2, \quad \psi_0(y, z) = -\frac{\varepsilon_w}{\gamma} \sigma y^2 \sin(k_m y z) \exp(-\mathrm{i} \ln y/\sigma). \tag{56, 57}$$

Having determined the inviscid flow stream function, it follows that the

companion velocity is

$$V_0(y, z) = -\frac{\varepsilon_w}{\gamma}[M_b y^3 \cos(k_m yz)\mathbf{e}_y + \mathrm{i}y \sin(k_m yz)\mathbf{e}_z] \exp(-\mathrm{i}\Phi_0), \tag{58}$$

where $\Phi_0 = \ln y/\sigma$. Note that the ratio of the normal and axial velocity terms in equation (58) is of $O(M_b)$, as assumed in section 6.2 above.

6.5. VISCOUS CORRECTIONS

Subject to later justification, it is stated without proof that the velocity and vorticity solutions that incorporate viscous effects must possess the same z-dependence as their inviscid counterparts. After examining equations (57) and (58), this proposition is implemented by setting

$$V_z(y, z) = V_c(y) \sin(k_m yz) \exp(-\mathrm{i}\Phi_0), \quad \varpi(y, z) = \varpi_c(y) \sin(k_m yz) \exp(-\mathrm{i}\Phi_0), \tag{59, 60}$$

where viscous correction multipliers, V_c and ϖ_c, must be determined. After substitution into the full vorticity transport equation, given by equation (41), several terms cancel out. Balancing terms of $O(Sr^2)$, one gets, after much algebra,

$$\frac{\mathrm{d}\varpi_c}{\mathrm{d}y} - \varepsilon\sigma^{-3}y^{-3}(1 - \mathrm{i}\sigma)\varpi_c = 0 \quad \text{or} \quad \varpi_c = C \exp[-\xi y^{-2}(1 - \mathrm{i}\sigma)/2], \tag{61}$$

where the viscous parameter $\xi = \varepsilon/\sigma^3 = k_m^2/(M_b^3 Re)$ appears as a dynamic similarity parameter in control of the viscous correction multiplier. The vorticity boundary condition at the wall, given by equation (51), allows evaluating the integration constant C. The outcome is readily found to be

$$C = -\frac{\varepsilon_w}{\gamma} Sr \exp[\xi(1 - \mathrm{i}\sigma)/2]. \tag{62}$$

The corrected vorticity incorporating viscous effects can be finally formulated from equation (60), namely,

$$\varpi(y, z) = -\frac{\varepsilon_w}{\gamma} Sr \sin(k_m yz) \exp\{-\xi(y^{-2} - 1)/2 - \mathrm{i}Sr[\ln y - \xi\sigma^2(y^{-2} - 1)/2]\}. \tag{63}$$

Having completely resolved ϖ, the corrected velocity, V_c, can be extracted now from the momentum equation relating velocity and vorticity, as expressed by equation (39). After some algebra, one finds

$$V_c = -\frac{\varepsilon_w}{\gamma}\left[\sigma y + \frac{\varepsilon}{\sigma^2 y} + \mathrm{i}\left(y - \frac{\varepsilon}{\sigma y}\right)\right](1 + \sigma^2)^{-1} \times \exp[-\xi(y^{-2} - 1)/2 + \mathrm{i}\xi\sigma(y^{-2} - 1)/2]. \tag{64}$$

The corrected axial component of the solenoidal velocity vector can be obtained

thereafter from equation (59):

$$V_z = -\frac{\varepsilon_w}{\gamma}\mathrm{i}\frac{[y - \xi\sigma^2 y^{-1} - \mathrm{i}(\sigma y + \xi\sigma y^{-1})]}{1+\sigma^2}\sin(k_m yz)\exp[-\zeta(y) + \mathrm{i}\sigma\zeta(y) - \mathrm{i}\Phi_0(y)], \tag{65}$$

where

$$\zeta(y) = \xi\int_1^y U_y^{-3}\,\mathrm{d}y = \xi(y^{-2}-1)/2. \tag{66}$$

Backward substitution into equation (27) yields

$$\tilde{u}_z(y, z, t) = \frac{\varepsilon_w}{\gamma}\mathrm{i}B\sin(k_m yz)\exp[-\zeta(y) - \mathrm{i}\varphi(y, t)], \tag{67}$$

where

$$B \equiv B^r + \mathrm{i}B^i, \quad B^r = (-y + \xi\sigma^2 y^{-1})/(1+\sigma^2), \quad B^i = \sigma(y + \xi y^{-1})/(1+\sigma^2), \tag{68}$$

and

$$\varphi(y, t) = k_m t + \Phi_0(y) - \sigma\zeta(y). \tag{69}$$

In the real domain, equation (67) can be recast into

$$\tilde{u}_z(y, z, t) = -\frac{\varepsilon_w}{\gamma}(B^i\cos\varphi - B^r\sin\varphi)\sin(k_m yz)\exp(-\zeta). \tag{70}$$

Thus, the total time-dependent axial velocity component can be constructed via equation (16), rendering

$$u_z^{(1)}(y, z, t) = \frac{\varepsilon_w}{\gamma}[\sin(k_m z)\sin(k_m t) - (B^i\cos\varphi - B^r\sin\varphi)\sin(k_m yz)\exp(-\zeta)] + O(Sr^{-1}), \tag{71}$$

in which the reported order of the truncation error will be verified in section 7.5 below.

6.6. NORMAL VELOCITY

The normal component $\tilde{u}_y$ can be determined in a manner to satisfy the conservation of mass principle. To that end, $\tilde{u}_z$ is used in the continuity equation, expressed by equation (22), while an *ansatz* is proposed for $\tilde{u}_y$. Beginning with

$$\tilde{u}_y(y, z, t) = \frac{\varepsilon_w}{\gamma}G(y)\cos(k_m yz)\exp[-\zeta(y) - \mathrm{i}\varphi(y, t)], \tag{72}$$

the unknown function $G(y)$ must be determined to satisfy continuity. Substituting equations (67) and (72) into equation (22), the spatial function $G(y)$ is extracted in a manner to ensure that $\partial\tilde{u}_y/\partial y = -\partial\tilde{u}_z/\partial z$ is satisfied in the

leading order terms. This occurs when

$$G(y) = M_b B y^2, \tag{73}$$

rendering

$$\tilde{u}_y(y, z, t) = \frac{\varepsilon_w}{\gamma} M_b y^2 B \cos(k_m y z) \exp[-\zeta(y) - \mathrm{i}\varphi(y, t)]. \tag{74}$$

Clearly, the original assumption of $\tilde{u}_y/\tilde{u}_z = O(M_b)$—leading to equation (39)—is justifiable. Furthermore, numerical computations of $\tilde{u}_y$ indicate that equation (74) is indeed accurate. Since comparisons with numerical predictions of $\tilde{u}_y$ can be easily drawn, they are omitted here for brevity.

7. DISCUSSION

Having successfully attained asymptotic formulations for both velocity and vorticity fields, the purpose of this section is to discuss the analytical results. The forthcoming discussion addresses two main topics: (1) the elucidation of essential features associated with the asymptotic derivation, and (2) the assessment of the global error associated with the final expressions. This includes an explanation of the solution type and character, an error analysis, a limit process verification in the event of no mean flow transmission, and a description of the intricate acoustico-vortical coupling established inside the cavity.

7.1. TOTAL TIME-DEPENDENT VELOCITY

Due to the small relative amplitude of $u_y^{(1)}$, the total time-dependent velocity component $u^{(1)}$ is prescribed by the axial component $u_z^{(1)}$ to $O(M_b)$. From equation (71), one can infer that

$$u^{(1)}(y, z, t) = \frac{\varepsilon_w}{\gamma}\left[\overbrace{\sin(k_m z)\sin(k_m t)}^{\text{acoustic part}} - \overbrace{(B^i \cos\varphi - B^r \sin\varphi)\sin(k_m y z)\exp(-\zeta)}^{\text{solenoidal part}}\right] + O(M_b). \tag{75}$$

The total time-dependent velocity comprises a juxtaposition of both acoustic and rotational velocity components. The rotational part is controlled by the viscous damping function ζ which causes it to depreciate more rapidly with larger damping parameters. This indicates that the rotational region and corresponding boundary layer thickness are reduced when $\xi = \nu_0 \omega_0^2 H/V_b^3$ is augmented. This, of course, can be accomplished in one of four different ways: by decreasing the normal velocity at the transpiring surface, or by increasing viscosity, frequency, or chamber width. When sufficiently removed from the transpiring wall, the rotational part vanishes, and the acoustic part dominates. Hence, near the core, the field is prescribed solely by the acoustic wave.

The normalised velocity ($\gamma u^{(1)}/\varepsilon_w$) is depicted in Figure 2 for the first four oscillation modes corresponding to a fundamental Strouhal number of 20 and a kinetic Reynolds number of 10^6. The axial station is chosen to coincide with the

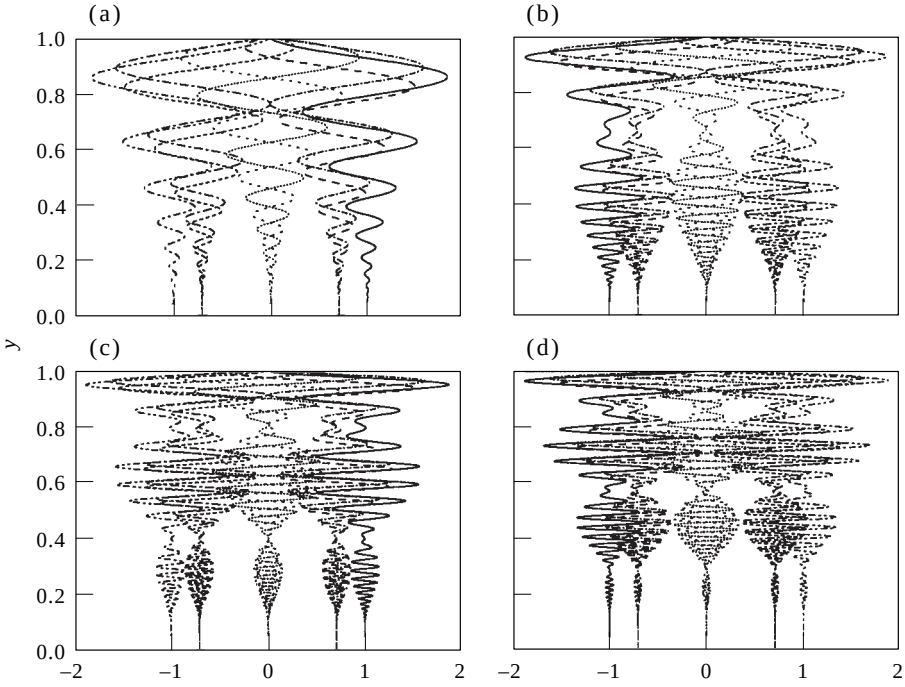

Figure 2. Numerical and analytical time-evolutions of the normalised velocity ($\gamma u^{(1)}/\varepsilon_w$) shown at the last pressure nodes, where $z^*/L = (2m-1)/(2m)$, and (a) $m = 1$, (b) $m = 2$, (c) $m = 3$, and (d) $m = 4$. Here $Sr = 20m$ and $Re_k = 10^6 m$. To the accuracy of the graph, numerical and analytical predictions are indistinguishable. Timelines correspond to eight evenly space values of $k_m t$ expressed in degrees: ——, 0; - - - - - -, 45; · · · · · ·, 90; –·–·–·–, 135; -··-··-··, 180; - - - - - -, 225; ·····, 270; -·-·-·-·-·-, 315.

last acoustic pressure node, where acoustic velocity amplitudes are largest, in order to bring into perspective some distinguished characteristics of the flow field. Evidently, the instantaneous velocity traces, separated by 45° in a period, describe a family of harmonic waves travelling from the transpiring wall to the core. They are characterised by a velocity overshoot near the wall and by a spatial wavelength that diminishes at higher oscillation modes. As shown in Figures 2 (b)–(d), the rotational velocity component is observed to vanish prematurely and then recuperate $(m-1)$ times. This peculiar phenomenon, which will be addressed subsequently, can be attributed to the downstream convection of zero vorticity lines that leave their imprints on the rotational field while passing by.

In Figure 2, note the striking resemblance that exists between analytical points generated from equation (75) and computational data obtained from numerical simulations of the governing differential equations of motion—achieved using a step size of 10^{-6} and a nine-stage Runge–Kutta scheme that exhibits a global error of order seven [11]. This agreement, which causes numerical and analytical results to become indistinguishable at all nine timelines, can be attributed to the small error associated with the analytical derivation and will be examined more closely in section 7.5.

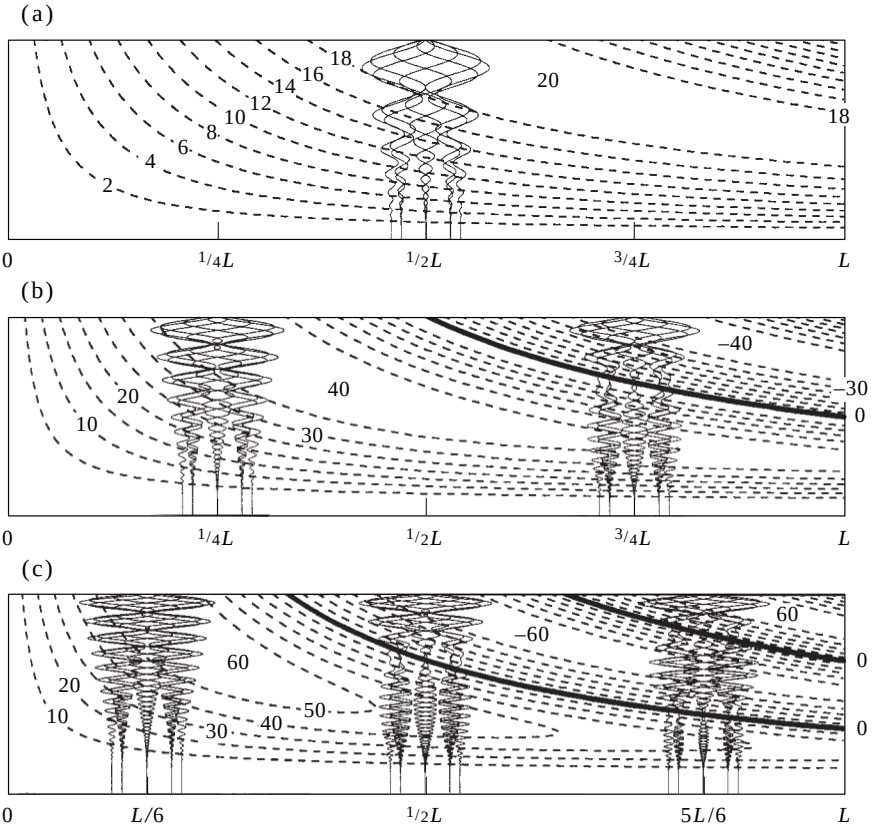

Figure 3. Velocity time-evolutions located at acoustic pressure nodes and overlaying vorticity contour lines shown for (a) $m = 1$, (b) $m = 2$, and (c) $m = 3$. Here $Sr = 20m$ and $Re_k = 10^6 m$.

7.2. ACOUSTICALLY–DRIVEN VORTICITY DISTRIBUTION

For the same test case parameters employed previously, Figure 3 shows the velocity profiles at pressure nodes when traced over iso-vorticity lines generated throughout the enclosure. Iso-vorticity lines produced from equation (63) indicate vortical intensification that scales with the Strouhal number near pressure nodes where local pressure gradients that are perpendicular to the particle inflow direction are largest. Clearly, vorticity that originates at pressure nodes is subsequently convected downstream by the bulk fluid motion. For second and third oscillation modes, Figures 3(b) and (c) show zones of reversed particle rotation separated by zero vorticity lines that emanate from acoustic velocity nodes. As irrotational streaks transport idle particles downstream, they cause zero vortical amplitudes to appear in the local velocity profiles that they happen to intersect. In a sense, the overall vorticity structure is dictated, first, by the acoustic wave character, and, second, by the convective mean flow motion.

7.3. THE RICHARDSON VELOCITY OVERSHOOT

A distinguishing mark of the time-dependent velocity is the existence of a velocity overshoot in the vicinity of the transpiring wall that can be attributed to

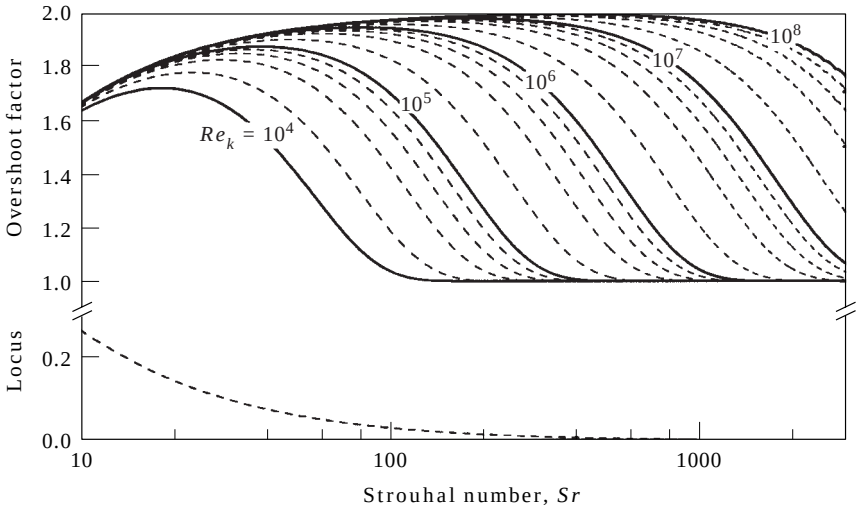

Figure 4. Locus and magnitude of the Richardson velocity overshoot for a wide range of control parameters and $z^*/L = 1/2$.

the phase difference between acoustic and vortical waves. This phase difference can cause the acoustic and vortical amplitudes to add up in a manner to result in a total amplitude that is almost twice the local acoustic wave amplitude. This, of course, can only happen near the wall, where the vortical amplitude is still large by virtue of its proximity to the wall where both vortical and acoustical wave amplitudes are equal. This phenomenon, referred to at times as "Richardson's annular effect", is a reassuring characteristic feature of oscillatory flows. First reported by Richardson [12] in experiments on sound waves in resonators, it was later verified theoretically by Sexl [13] and confirmed by Richardson and Tyler [14] in additional experiments conducted on reciprocating flows driven by pure periodic motions and in the absence of any mean flow transmission. The originality of the current analysis is that it involves an oscillatory field over a transpiring wall which induces much higher overshoot factors. As shown in Figure 4, overshoot factors ranging from 100 to 200% of the acoustic wave amplitude are possible for various physical parameters. In particular, decreasing viscosity or increasing the kinetic Reynolds number leads to large overshoot factors. For the same Re_k, decreasing the blowing speed V_b brings the model closer to the hardwall case exhibiting an infinite Strouhal number. As one would expect, this is conducive of attenuated overshoot factors.

For the same wide range of control parameters, the locus of this overshoot is shown in Figure 4 on a different scale in fractions of the distance from the wall. Clearly, the locus occurs in the upper 25% of the solution domain adjacent to the wall and is independent of viscosity or the kinetic Reynolds number. This can be attributed to the strong convective currents which, along with inertia, constitute the dominant forces near the wall. In a sense, the role played by viscosity becomes locally secondary, and is deferred to a "blown-off" viscous layer that is described quite adequately by Cole and Aroesty [15] in the analysis of steady flows over permeable walls with sidewall injection. As the Strouhal

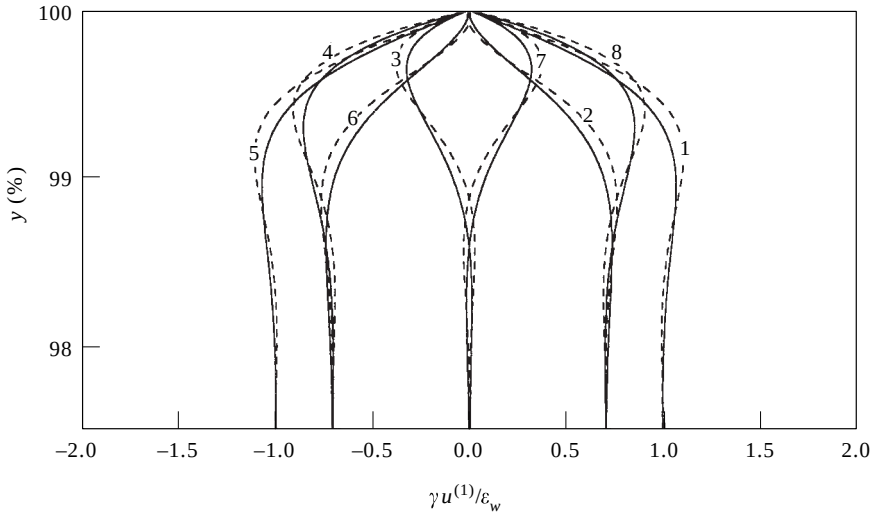

Figure 5. Comparison to the Stokes exact hardwall solution recuperated by suppressing the transverse mean flow velocity. Profiles are shown at eight successive times (labeled 1–8) that are separated by a phase difference of 45°: ——, exact ($V_b = 0$); - - - - - -, asymptotic. Here $Re_k = 10^5$, $\xi = \lambda_S = 224$, $z^*/L = 1/2$, and $m = 1$.

number is increased, with the effect of bringing the model closer to the hardwall case, the overshoot loci approach the wall, in compliance with conventional theory, since hardwall oscillations exhibit much thinner rotational layers.

7.4. THE HARDWALL CASE

In a limiting-process validation attempt, the normal convection speed V_b at the wall is reduced below the Stokes diffusion speed, $V_d = \sqrt{2\omega_0\nu_0}$, which is usually a very small quantity. With regards to the control parameters, this is found to coincide with a threshold case corresponding to $\xi = \lambda_S$, where $\lambda_S = H\sqrt{\omega_0/2\nu_0}$ is the Stokes number. On that account, predictions from equation (75) are compared with the classic, exact velocity profile derived for a harmonic pressure wave between impermeable, parallel plates [7] in Figure 5. Since V_d is practically very small, the test case presented here sets the lower limit for V_b in the current model.

7.5. ERROR ANALYSIS

The concurrence of analytical and numerical predictions in Figure 2 is not merely fortuitous since it can be attributed to the relatively small maximum error incurred in the asymptotic expansion. In order to determine the order of this error, and by way of insuring the accuracy reported in the aforementioned formulations, a strategy described by Bosley [16] is invoked. To that end, first define

$$\underset{0\leqslant y\leqslant 1}{E_{max}}\,(y,\, Re_k,\, Sr) = |u^{(1)}_{\text{numerical}} - u^{(1)}_{\text{analytical}}|_{max} \tag{76}$$

to be the maximum absolute discrepancy over the solution interval between the

numerical outcome of equation (11) achieved using a seventh order Runge–Kutta scheme and a subinterval of 10^{-6}, and the asymptotic formulation given via equation (71). Then show that the maximum absolute error exhibits the classical logarithmic form,

$$E_{max} = KSr^{-\kappa}, \tag{77}$$

by determining the order of the error κ from the slope of the linear least-squares fit to the data sets corresponding to log E_{max} plotted versus log Sr for different values of Re_k. Recalling that E_{max} represents the total or global truncation error, results are summarised in Figure 6(a) where the maximum error is calculated at several discrete values of Re_k. In most physical settings corresponding to $Re_k > 5 \times 10^5$, the *maximum* error is practically insignificant, being of the order of a few percent. This explains the excellent agreement with numerical simulations reported previously.

In addition to the slopes obtained from a least-squares linear curve fitting analysis, it can be graphically inferred from Figure 6 that the order of the error approaches one asymptotically for large Re_k. In other words,

$$\kappa \underset{\substack{1/Sr \to 0 \\ 1/Re_k \to 0}}{\longrightarrow} 1, \tag{78}$$

which confirms that the truncation error reported for equation (71) is of $O(Sr^{-1})$. This is further verified in Figure 6(b) showing in a plot of E_{max} versus Re_k that $E_{max} \sim 1/Sr$ for large Re_k.

7.6. COMPARISON TO EXPERIMENTAL FINDINGS

A qualitative agreement may be said to exist between the current theoretical formulation and experimental observations made by Ma *et al.* [1–3] and Barron *et al.* [4, 5]. Insofar as the wave character is concerned, these experiments tend to

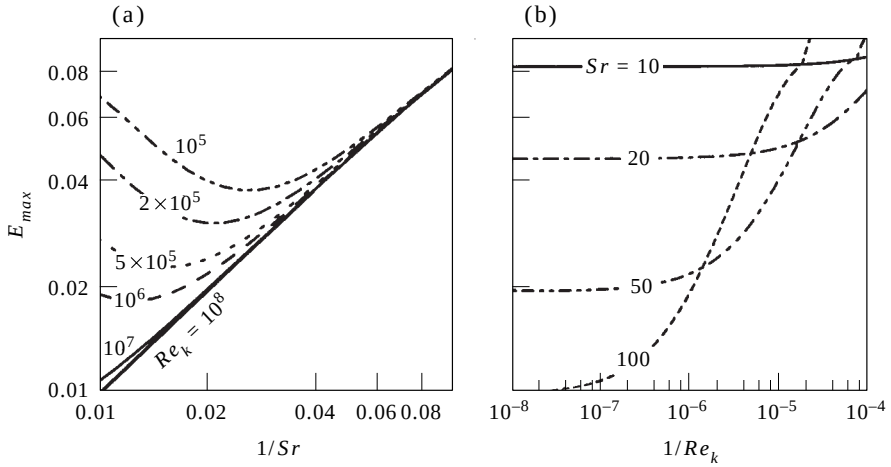

Figure 6. Asymptotic behaviour of the maximum error for variations in (a) Sr at constant Re_k, and (b) Re_k at constant Sr.

confirm the main vortical features described above. For example, the additional vortical component near the wall, leading to a pronounced velocity overshoot, has indeed been reported in references [4, 5] and alluded to in references [1–3]. The exponential rate of decay of the wave amplitude, borne out in equation (75), is also in qualitative agreement with the hot-wire measurements recorded in the cold-flow investigations by Ma and Barron. As predicted by the current analytical solution, the vortical element seems to disappear away from the walls, where the purely acoustic field is seen to persist. Further experimental details are furnished in reference [5].

8. CONCLUSIONS

In this report, regular perturbation expansions of the linearised Navier–Stokes equations are shown to lead to closed-form formulations of the velocity and vorticity fields inside a rectangular enclosure. The enclosure accommodates a strong coupling between the classic cavity mean flow and the internal acoustic environment. Accurate, uniformly valid asymptotic expressions are obtained that agree very well with numerical predictions. The time-dependent velocity comprises both acoustic and vortical wave components and exhibits several characteristics of oscillatory flows. These include a classical wave depreciation and a velocity overshoot in the vicinity of the wall. New characteristic features include intense velocity overshoot factors reaching almost twice the acoustic wave amplitude, and nodes of zero rotational velocity amplitudes occurring downstream of velocity node stations. These rotational velocity nodes appear for harmonic oscillation modes only, owing to the downstream convection of zero vorticity lines that emanate from acoustic velocity node stations. The vortical structure is closely intertwined with the mean and acoustic wave characters and exhibits interesting features as well. Unsteady vorticity amplitudes are found to scale with the Strouhal number and are largest when originating from acoustic pressure nodes where pressure gradients parallel to the permeable wall are largest. Subsequently, vorticity lines are transported downstream by the bulk fluid action. In the limiting process when the convection speed is suppressed below the speed of diffusion, the approximate formulation reduces asymptotically to the Stokes exact solution for an oscillatory field over a rigid wall. The few percent in global error incurred throughout the derivation process are found to diminish with decreasing friction or viscosity.

REFERENCES

1. Y. Ma 1990 *Ph.D. thesis*, *University of Utah*, *Salt Lake City*, *UT*. A simulation of the flow near a burning propellant in a solid propellant rocket motor.
2. Y. Ma, W. K. Van Moorhem and R. W. Shorthill 1990 *Journal of Vibration and Acoustics—Transactions of the ASME* **112**, 550–555. Innovative method of investigating the role of turbulence in the velocity coupling phenomenon.
3. Y. Ma, W. K. Van Moorhem and R. W. Shorthill 1991 *Journal of Propulsion and Power* **7**, 692–699. Experimental investigation of velocity coupling in combustion instability.

4. J. BARRON 1997 *Ph.D. thesis*, *University of Utah*, *Salt Lake City*, *UT*. The onset of turbulence in a simulation of the oscillating flow over a burning propellant.
5. J. BARRON, J. MAJDALANI and W. K. VAN MOORHEM 1998, *AIAA. Paper No.* 98-2694, *Albuquerque*, *NM*. A novel investigation of the oscillatory field over a transpiring surface.
6. M. VAN DYKE 1975 *Perturbation Methods in Fluid Mechanics*. Stanford, CA: The Parabolic Press.
7. F. M. WHITE 1991 *Viscous Fluid Flow*. New York: McGraw-Hill.
8. A. SOMMERFELD 1950 *Mechanics of Deformable Bodies*. New York: Academic Press.
9. B. T. CHU and L. S. G. KOVÁSZNAY 1957 *Journal of Fluid Mechanics* **3**, 494–514. Nonlinear interactions in a viscous heat-conducting compressible gas.
10. G. A. FLANDRO 1974 *Journal of Sound and Vibration* **36**, 297–312. Solid propellant acoustic admittance corrections.
11. J. C. BUTCHER 1987 *The Numerical Analysis of Ordinary Differential Equations*. Chichester: Wiley.
12. E. G. RICHARDSON 1928 *Proceedings of the Physical Society*, *London* **40**, 206–220. The amplitude of sound waves in resonators.
13. T. SEXL 1930 *Zeitschrift für Physik* **61**, 349–362. Über den von E.G. Richardson entdeckten 'Annulareffekt'.
14. E. G. RICHARDSON and E. TYLER 1929 *Proceedings of the Royal Society, London* **A 42**, 1–15. The transverse velocity gradient near the mouths of pipes in which an alternating or continuous flow of air is established.
15. J. D. COLE and J. AROESTY 1968 *International Journal of Heat Mass Transfer* **11**, 1167–1183. The blowhard problem—inviscid flows with surface injection.
16. D. L. BOSLEY 1996 *SIAM Review* **38**, 128–135. A technique for the numerical verification of asymptotic expansions.

APPENDIX A: LINEARISED NAVIER–STOKES

Inserting the expanded variables into equation (1) yields

$$\partial(1+\rho^{(1)})/\partial t + \nabla\cdot[(1+\rho^{(1)})(M_b\mathbf{U}+\mathbf{u}^{(1)})] = 0, \tag{A1}$$

$$\nabla\cdot\left(M_b\underbrace{\mathbf{U}}_{O(\varepsilon_w^0)} + \underbrace{\mathbf{u}^{(1)}}_{O(\varepsilon_w^1)} + M_b\underbrace{\rho^{(1)}\mathbf{U}}_{O(\varepsilon_w^1)} + \underbrace{\rho^{(1)}\mathbf{u}^{(1)}}_{O(\varepsilon_w^2)}\right) + \partial\rho^{(1)}/\partial t = 0. \tag{A2}$$

Collecting terms to the first order in the wave amplitude, and ignoring smaller terms, one gets

$$\partial\rho^{(1)}/\partial t + \nabla\cdot(\mathbf{u}^{(1)} + \rho^{(1)}M_b\mathbf{U}) = 0, \tag{A3}$$

which is equation (10). Inserting the expanded variables into equation (2), and recalling that $\nabla\cdot\mathbf{U} = 0$, one gets

$$\rho\partial\mathbf{u}/\partial t = (1+\rho^{(1)})\partial(M_b\mathbf{U}+\mathbf{u}^{(1)})/\partial t = \partial\mathbf{u}^{(1)}/\partial t + \rho^{(1)}\partial\mathbf{u}^{(1)}/\partial t, \tag{A4a}$$

$$\begin{aligned}\mathbf{u}\cdot\nabla\mathbf{u} &= (M_b\mathbf{U}+\mathbf{u}^{(1)})\cdot\nabla(M_b\mathbf{U}+\mathbf{u}^{(1)})\\ &= M_b^2\mathbf{U}\cdot\nabla\mathbf{U} + M_b\mathbf{U}\cdot\nabla\mathbf{u}^{(1)} + M_b\mathbf{u}^{(1)}\cdot\nabla\mathbf{U} + \mathbf{u}^{(1)}\cdot\nabla\mathbf{u}^{(1)}.\end{aligned} \tag{A4b}$$

$$\rho\mathbf{u}\cdot\nabla\mathbf{u} = (1+\rho^{(1)})\mathbf{u}\cdot\nabla\mathbf{u} = M_b^2\mathbf{U}\cdot\nabla\mathbf{U} + M_b\mathbf{U}\cdot\nabla\mathbf{u}^{(1)} + M_b\rho^{(1)}\mathbf{u}^{(1)}\cdot\nabla\mathbf{U}$$
$$+ M_b^2\rho^{(1)}\mathbf{U}\cdot\nabla\mathbf{U} + \rho^{(1)}\mathbf{u}^{(1)}\cdot\nabla\mathbf{u}^{(1)} + M_b\mathbf{u}^{(1)}\cdot\nabla\mathbf{U} + \mathbf{u}^{(1)}\cdot\nabla\mathbf{u}^{(1)}$$
$$+ M_b\rho^{(1)}\mathbf{U}\cdot\nabla\mathbf{u}^{(1)} \tag{A4c}$$

$$-\nabla p/\gamma = -\nabla p^{(1)}/\gamma, \tag{A4d}$$

$$Re^{-1}[4\nabla(\nabla\cdot\mathbf{u})/3] = 4Re^{-1}\nabla[\nabla\cdot(M_b\mathbf{U}+\mathbf{u}^{(1)})]/3 = 4Re^{-1}\nabla(\nabla\cdot\mathbf{u}^{(1)})/3, \tag{A4e}$$

$$-Re^{-1}\nabla\times(\nabla\times\mathbf{u}) = -Re^{-1}\nabla\times[\nabla\times(M_b\mathbf{U}+\mathbf{u}^{(1)})]$$
$$= -Re^{-1}M_b\nabla\times(\nabla\times\mathbf{U}) - Re^{-1}\nabla\times(\nabla\times\mathbf{u}^{(1)}). \tag{A4f}$$

Adding up equations (A4a)–(A4f), one realises that the zero order terms yield back equation (9) associated with the steady field. Collecting terms to the first order in the wave amplitude, and disregarding smaller terms, one obtains

$$\partial\mathbf{u}^{(1)}/\partial t + M_b\mathbf{U}\cdot\nabla\mathbf{u}^{(1)} + M_b\mathbf{u}^{(1)}\cdot\nabla\mathbf{U}$$
$$= -\nabla p^{(1)}/\gamma + 4Re^{-1}\nabla(\nabla\cdot\mathbf{u}^{(1)})/3 - Re^{-1}\nabla\times(\nabla\times\mathbf{u}^{(1)}), \tag{A5}$$

which by making use of the identity,

$$(\mathbf{U}\cdot\nabla)\mathbf{u}^{(1)} + (\mathbf{u}^{(1)}\cdot\nabla)\mathbf{U} = \nabla(\mathbf{u}^{(1)}\cdot\mathbf{U}) - \mathbf{u}^{(1)}\times(\nabla\times\mathbf{U}) - \mathbf{U}\times(\nabla\times\mathbf{u}^{(1)}),$$

leads to the leading order, time-dependent momentum equation, referred to in section 2 as equation (11).